The Capabilities of Defocused Digital Particle Image Velocimetry

Emilio Castaño Graff, Francisco Pereira, Michele Milano, Mory Gharib

Abstract Defocused Digital Particle Image Velocimetry, or DDPIV, is the direct extension of DPIV into the third spatial dimension. Capabilities of DDPIV include surface tracking, particle sizing, and flow velocity measurements, all of which can be performed simultaneously in a properly set-up experiment. Because the measurement domain of a DDPIV camera is a volume (as opposed to a plane as in SPIV), spatial derivatives can be calculated along the X, Y, and Z directions. Additionally, if the flow at hand evolves appropriately with respect to the sampling frequency, time derivatives can be calculated. As compared with photogrammetric techniques, DDPIV cameras are a single assembled unit and thus in most cases they need only be calibrated at assembly time with the exception of the particle sizing function which requires an in-situ calibration.

1 Introduction

Over the past 30 years, particle image velocimetry has evolved into a widely accepted flow diagnostic tool. The advent of commercially available digital imagers simplified the acquisition method (Cho 1989, Willert and Gharib 1991) and the analysis methods evolved accordingly (Keane and Adrian 1992, Westerweel 1997).

Stereo DPIV allowed the third component of velocity to be extracted from two views of a planar domain (Gauthier and Riethmuller 1988), and evolved into the now frequently used Scheimpflug arrangement (Prasad and Jensen 1995). To extract the depth derivative the technique has been extended to multiple planes (Kähler and Kompenhans 2000). However, it remains a planar technique and thus the spatial derivatives are difficult to estimate without complex optical setups. The complexity of the optical train in holographic techniques has made this volumetric technique somewhat undesirable.

Defocusing Digital Particle Image Velocimetry combines the simplicity of DPIV with the desirability of the volumetric measurement domain. The method reconstructs three-dimensional point clouds from digital images and thus it has the added advantage of being able to track marked surfaces and perform particle sizing (the sizing is absolute with an in-situ calibration). The simplicity of DPIV is maintained in that the imaging unit is one-piece and in normal conditions requires only calibration at the time of manufacture. The light source need only illuminate the seed particles in the appropriate volume and thus its alignment to the camera is much less sensitive.

2 The Defocusing Concept and Basic Theory

A point in space off-axis from an aperture will have an image that experiences a lateral offset as the point moves along the axis of the optical system. The defocusing technique embraces this phenomenon and images each point in space through multiple apertures. With knowledge of the basic optical parameters of the system, the relative shift between images can be used to calculate the out-of-plane position of each point. Each defocused particle in space will generate multiple images that form a pattern corresponding to the shape of the aperture layout, but at varying scales (dependent on the distance from the point to the reference plane). In processing the images, it is then necessary to look at all the particle images and find the corresponding images that together complete the aperture layout pattern. Although only two apertures are required to extrapolate the three-dimensional position of a point, in practice at least three apertures are necessary to decrease the number of mismatched particle images ("ghost" particles). Each subsequent aperture added ever decreasingly reducing the position error and the number of ghost particles.

Emilio Castaño Graff, Michele Milano, Mory Gharib
Graduate Aeronautical Laboratories at the California Insitute of Technology, Pasadena, California, USA

Francisco Pereira
INSEAN, Rome, Italy

Correspondence to:
Emilio Castaño Graff
E-mail: pelesl@its.caltech.edu

The term "defocusing" in this case is not associated with the blur inherent in the image of a point not on the focal plane of the system. DDPIV does not rely on the image blur to extrapolate the spatial position of a point source, and the entire concept can be explained using pin-hole optics arguments (which imply an infinite depth of field). In practice, the image blur plays a role in the estimation of the sub-pixel location of the particle images. Using separate sensors for each aperture allows for an increase in the aperture separation (without the prohibitive cost of enormous lenses) and for particle image separation so that the particle image matching becomes less ambiguous. Another advantage of separating the aperture spaces is that the seeding density can be much higher than if all apertures formed images on the same sensor.

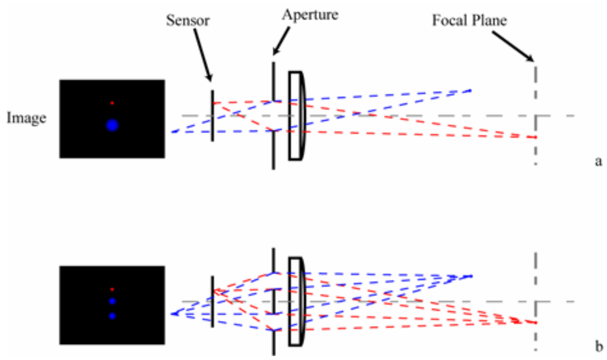

Figure 1: A schematic of the defocusing concept. Figure *a* depicts a standard, single-aperture optical system imaging a particle on the focal plane and one ahead of it. The particle not on the focal plane appears as a blurred dot. Figure *b* depicts an optical system with two off-axis apertures, through which the out-of-focus point forms two blurred images. The distance between them is directly related to the characteristics of the optical system (focal length, aperture separation, and distance to the focal plane) and the spatial position of the point source.

The theory behind the imaging system for DDPIV is covered intensively in Pereira and Gharib 2002. Here we present a slightly more generalized form and equate it with the previous work.

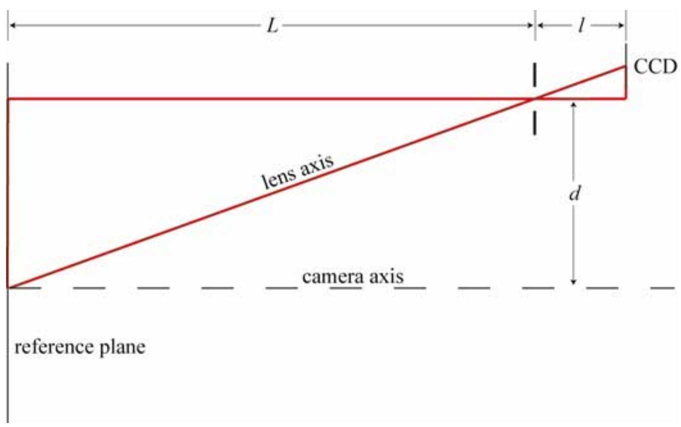

Figure 2: A schematic of sensor alignment with respect to the DDPIV camera axis and reference plane

The arrangement of the multiple sensor/lens systems in a DDPIV camera is such that, at the reference plane, all sensors have an exactly equal field of view, and all apertures are coplanar. This condition is shown in figure 2 for one sensor with the optics replaced by a single aperture. The position of the aperture relative to the DDPIV optical axis (c, d) is a design parameter as is the value of L, the distance from the aperture plane to the reference plane.

Knowing the focal length of the lens f the distance l is calculated by the thin lens equation:

$$\frac{1}{L}+\frac{1}{l}=\frac{1}{f}\Rightarrow l=\frac{Lf}{L-f} \tag{1}$$

With the origin at the intersection of the DDPIV optical axis and the aperture plane, using pinhole optics arguments specify that the position of the center of the sensor in space has coordinates

$$X_C = c\left(1+\frac{f}{L-f}\right),\ Y_C = d\left(1+\frac{f}{L-f}\right),\ Z_C = -\frac{fL}{L-f} \tag{2}$$

where c and d are the coordinates of the corresponding aperture relative to the system single optical axis. If the sensor is perfectly aligned (it has center with coordinates as defined by equation 2 and is parallel to the aperture plane) then it can be shown that a point in space with coordinates (X_P, Y_P, Z_P) has image coordinates

$$x = \frac{f}{L-f}\frac{c(L-Z_P)-LX_P}{Z_P},\ y = \frac{f}{L-f}\frac{d(L-Z_P)-LY_P}{Z_P} \tag{3}$$

Given two apertures *i* and *j*, the separation between the particle images is

$$b_{ij} = M\,\frac{L-Z_P}{Z_p}s_{ij} \tag{4}$$

Here, *M* is the optical magnification as defined by pinhole optics and *s* is the separation between apertures *i* and *j*. Equation 4 represents mathematically the statement above that each point in space will be imaged as a pattern with the same shape as the aperture layout but at a scale corresponding to the depth of the point in space.

To maintain consistency with Pereira and Gharib 2002, we introduce the quantity *K*:

$$K = \frac{1}{Ms_{ij}L} \tag{5}$$

Now, we can rewrite the image separation (4) in the same form:

$$b_{ij} = \frac{1}{K}\left(\frac{1}{Z_P}-\frac{1}{L}\right) \tag{6}$$

Continuing from (4), the sensitivity of an aperture pair in Z is

$$\frac{\partial b_{ij}}{\partial Z_P} = -\frac{M}{Z_P^2}s_{ij} \tag{7}$$

The coordinates of the point in space can be calculated from its images from (4):

$$Z_P = \frac{L}{1+\frac{b_{ij}}{M}\frac{1}{s_{ij}}} \tag{8}$$

Knowing the Z coordinate of the point, the X and Y coordinates are the coordinates of the centroid of the image pattern, and can be written as:

$$X_P = \bar{c}\left(1-\frac{Z_P}{L}\right)-\bar{x}M\,\frac{Z_P}{L},\ Y_P = \bar{d}\left(1-\frac{Z_P}{L}\right)-\bar{y}M\,\frac{Z_P}{L} \tag{9}$$

where ($\bar{c}$, $\bar{d}$) are the coordinates of the matched pattern centroid.

3
DDPIV Systems in Practice

Even though the theory suggests that only two apertures are necessary, normally this is insufficient. The only robust way to match particle images together is the aperture layout pattern and thus having only two apertures leads to a likely chance of mismatch in dense fields. In practice DDPIV systems use three apertures arranged in an equilateral triangle. This arrangement guarantees that the sensitivity between any two apertures is equal. There are cases where this advantage can be sacrificed in favor of package size, as was done in the underwater system for full-scale field experiments on naval vessels. Sensors are typically double-exposure interline transfer CCD's as in many other PIV applications.

Figure 3: An underwater DDPIV system with a shortened aperture layout to reduce drag.

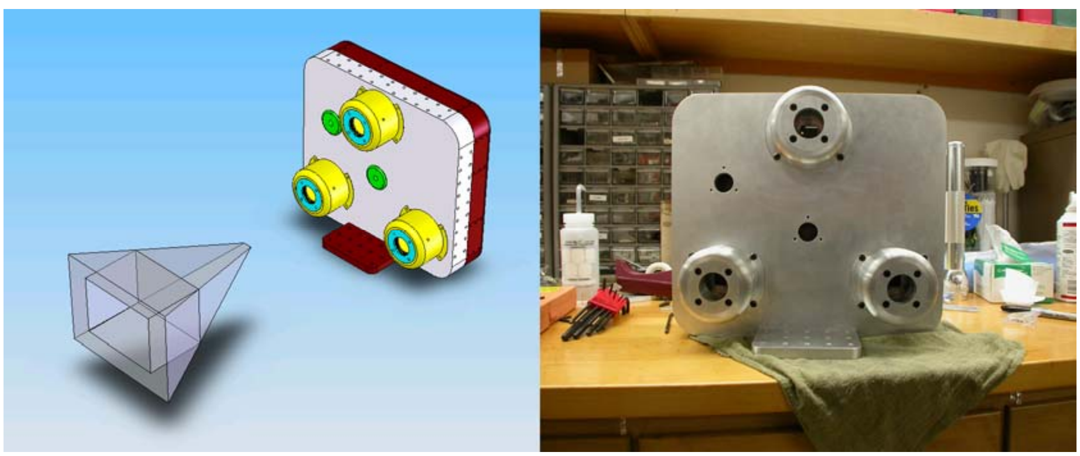

Figure 4: A latest-generation DDPIV camera. The CAD model shows a geometrical estimate of the measurement domain (the asymmetric pyramid). The "**characteristic volume**" – the number used to describe the measurement domain – is the side length of the largest rectangular prism inscribable within this pyramid-like shape.

Due to manufacturing tolerances and other factors, it is impossible for real systems to meet the conditions established in section 2. All real cameras require an initial calibration to correct for errors in the placement of the sensors and aberrations as well as differences in the lenses.

This calibration, or "multiplane dewarping", need only be performed at the time of assembly. The underwater system show in figure 3, for example, was calibrated once in-lab, then mounted to the transom of the R/V Athena for 3 12-hour trips to the Gulf of Mexico. Once it returned to the lab, it showed no loss in precision in the mapping of particle fields.

Multiplane dewarping consists of imaging several known grid planes throughout the volume. It is similar to calibrations commonly used for SPIV systems but differs in how the correction is applied to experimental data.

A target displaying a grid of dots with a calibrated spacing is translated across the desirable measurement volume along the depth-axis in a discretionary number of steps. At each Z-station, the target is imaged through the DDPIV camera. The system's mechanical and optical imperfections, (e.g. sensor misalignment, lens aberrations, flow setup such as windows and fluid media optical properties) are recorded as a distortion of the perfect calibration grid. The distorted dot coordinates are measured using sub-pixel techniques and are then associated to the perfect grid coordinates. A multi-parameter non-linear optimization is then performed to derive a family of best mapping functions, in the least-mean squares sense, between the distorted grid and the ideal grid. The process provides 2nd, 3rd and 4th order polynomial-type functions. A family of these functions is calculated independently for each calibration Z-station.

Experimental data is corrected using these calibration coefficients, but whereas most dewarping techniques apply to the images themselves, in the defocusing method the correction is applied to the particle image coordinates in two distinct stages. In a first stage, a coarse pattern matching is performed on the complete dataset using the calibration data obtained at one given plane (usually the reference plane), i.e. the particle image coordinates are corrected (or "dewarped") using one single mapping function. This coarse analysis provides a means to calculate a rough estimate of every single particle location in space, which is used to select the two nearest calibration stations for the second stage. The corresponding mapping functions are applied to the distorted particle image coordinates and a second and final pattern matching is performed using tighter tolerances. This two-stage process allows for a higher degree of accuracy in the measurement of the depth location Z, and reduces drastically the population of ghost particles.

In an experimental setting, the volume is illuminated by a pulsed light source, be it a laser or a strobe, and then the images are converted to three-dimensional point clouds. One can then apply a particle sizing calibration set to these fields to obtain absolute size, though relative size can be calculated without any additional calibration. Once each frame triplet is converted to a point cloud in space coordinates, the velocity can be calculated either by a three-dimensional cross-correlation (PIV) or, if the seeding density is appropriate, by three-dimensional particle tracking (PTV).

The resulting three-component volumetric vector fields contain a wealth of information. Spatial derivatives can be calculated in all three directions, thus quantities like vorticity and divergence can be calculated completely. The vorticity can be visualized either by isosurfaces or by streamlines, which in some sense correspond to vorticity lines. "Virtual dye" visualizations can be performed by computationally placing particles in the vector fields and integrating their paths in time.

4
Examples of the Capabilities of DDPIV

The performance and capability of DDPIV are demonstrated by a series of experiments performed with second-generation DDPIV cameras.

Bubble Sizing aft of the R/V Athena

The underwater DDPIV system, built originally for a field experiment aboard the R/V Revelle, was modified in the summer of 2004 to perform bubble sizing in two locations: directly aft of the port-side propeller and at the centerline of the hull of the R/V Athena (length of 50 meters with beam of 7 meters) of the Naval Sea Systems Command, Carderock Division. The fully sealed DDPIV camera was coupled rigidly via spaceframe to the fully sealed illumination optics. The acquisition system and laser head sat on deck near the transom of the ship. The characteristic volume of this camera is approximately 90mm.

Figure 5: The R/V Athena in its early days as a research vessel.

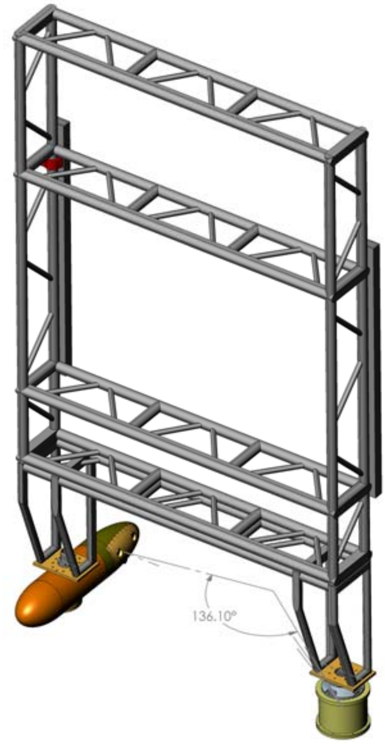

Figure 6: CAD model of the underwater DDPIV system for the R/V Athena. The camera is on the left, and the laser optics on the right, with an indication of the forward-scatter angle. The frame was mounted on rails that had been welded to the transom of the ship.

An in-situ sizing calibration was performed prior to each experimental run. This consisted of imaging a target replete with particles of known size and index of refraction with the underwater system. The calibration data generated from this set is a correlation between location in space, light intensity, and size which is used to infer particle size in the subsequent run (see Pereira and Gharib 2004).

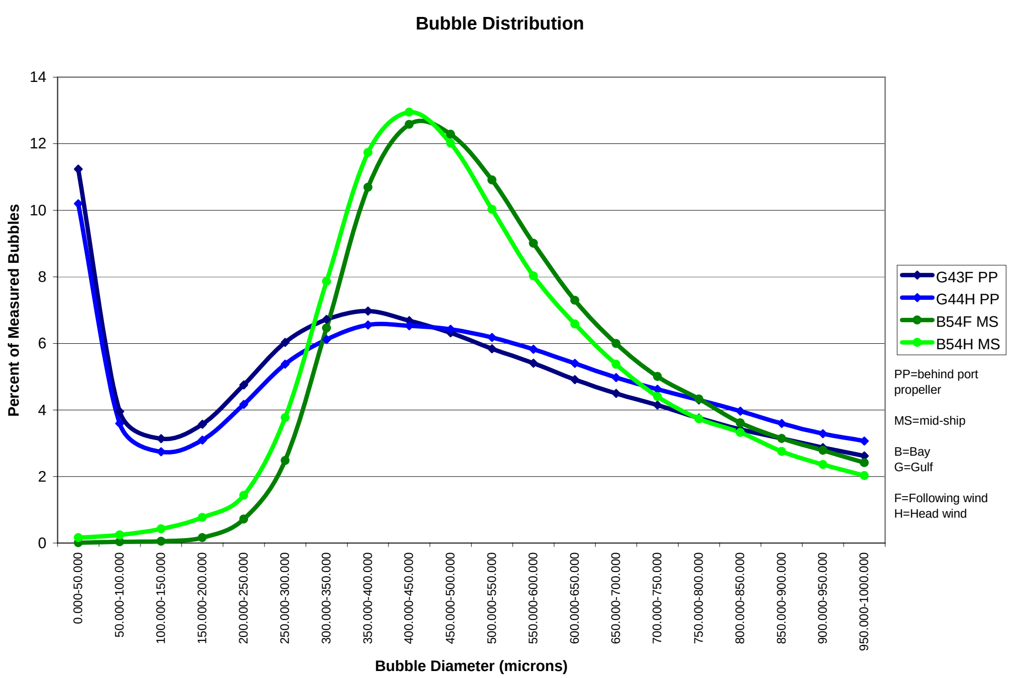

Flow around an Impulsively Started Plate

After returning from the field test aboard the R/V Athena, the same camera was used in the lab to visualize the flow in the wake of an impulsively started plate in water. The plate and camera were tied together so as to maximize the portion of the wake that could be imaged. The plate was submerged in water and the system was impulsively started normal to the span of the plate. Velocity was calculated with PIV.

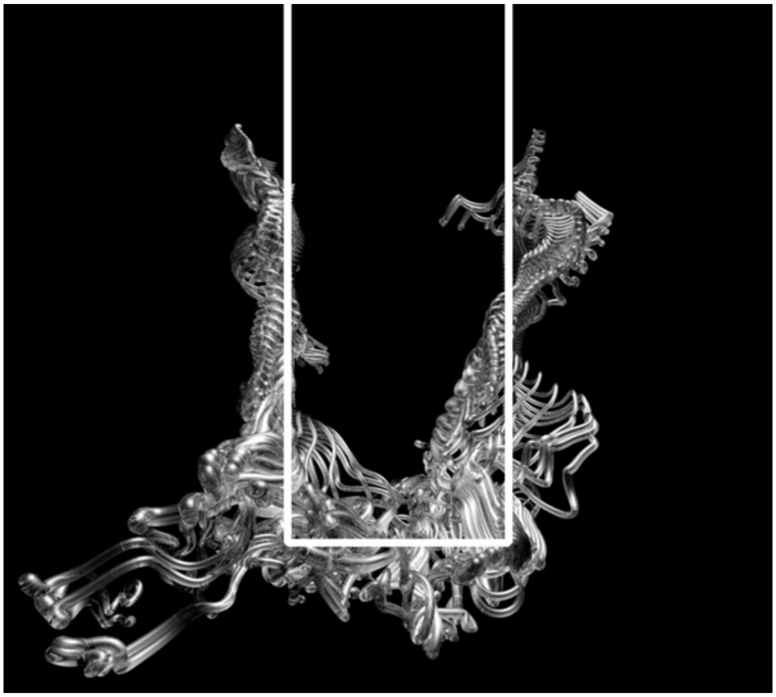

Figure 7: Virtual dye rendering of the streaklines of particles placed on the edge of the plate (highlighted in white). This is for a full (forward, then back) stroke composed of 20 phase-averaged vector fields with about 23 vectors to a side.

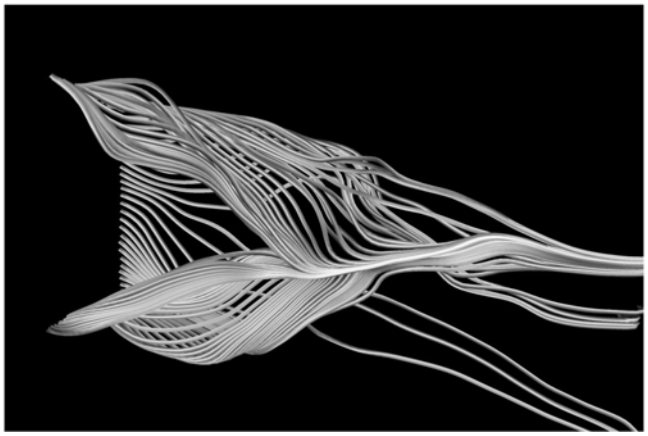

Figure 8: Streamlines of velocity in the wake of the plate as seen from above. The camera imaged the experiment from the right (relative to this picture).

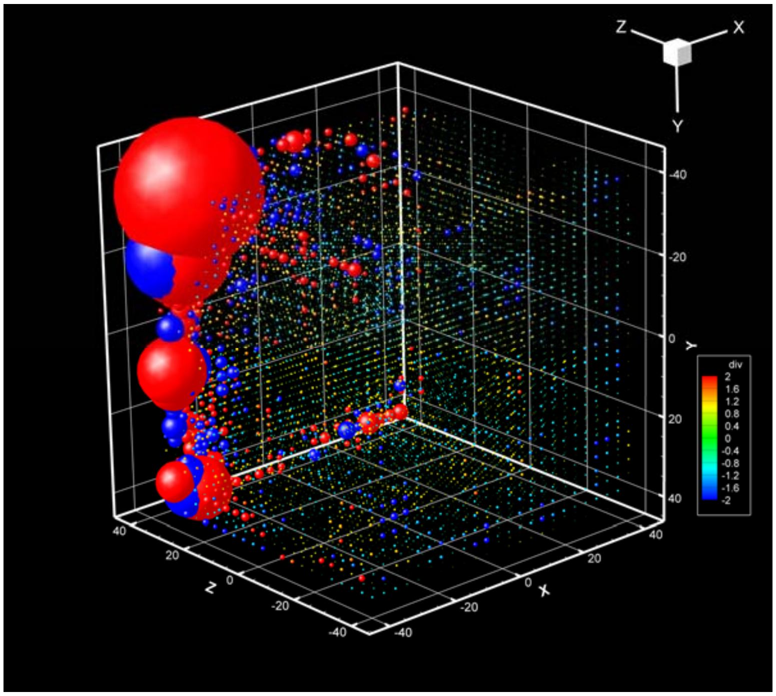

Figure 9: One frame of the divergence field of the plate data. The sphere size and color indicate the value of the divergence. In this example, noise vectors (frequently found at the edge of the domain) were left as comparison to the good data in the core of the volume. The average divergence in the core is on the order of 10^{-4}.

The flow was seeded using 80-micron-diameter fluorescent particles and illuminated by a pulsed Nd:YAG laser expanded into a cone perpendicular to the axis of the camera.

Flow around a Rigid Flap

A 40-millimeter-wide mechanical flapper powered by a small servomotor was made to flap continuously at ~1 Hertz in water seeded with 44-micron-diameter white polyurethane particles. Small imperfections on the black-anodized aluminum flap made it possible to track the position of the flap concurrently with the flow so that its position could be correlated more easily with the surrounding flow. Velocity was calculated with PIV.

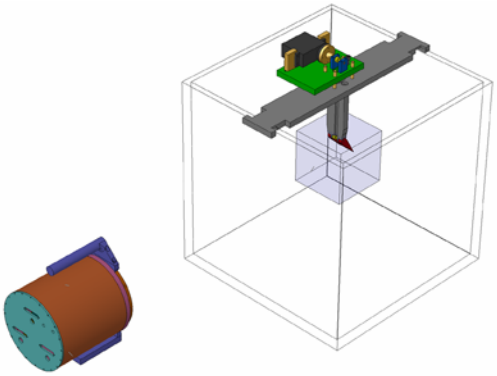

Figure 10: Experimental setup for the flap experiment, showing the DDPIV camera (lower left), the flap, the tank, and the approximate characteristic volume (light purple).

Once the flap reflections were isolated, it was easy to add a three-dimensional model of the flap to the vector fields to facilitate visualization. This capability is indispensable when studying flows involving moving boundaries.

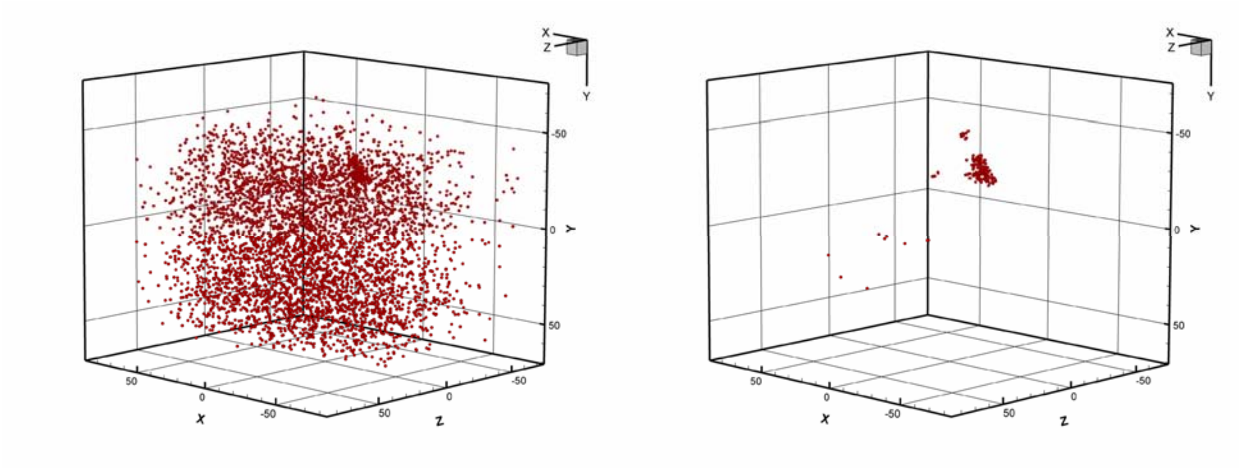

Figure 11: Sample particle field from the flap experiment. On the left, all the found particles are displayed. On the right, the flap is easily isolated by applying a density filter (number of closest neighbors).

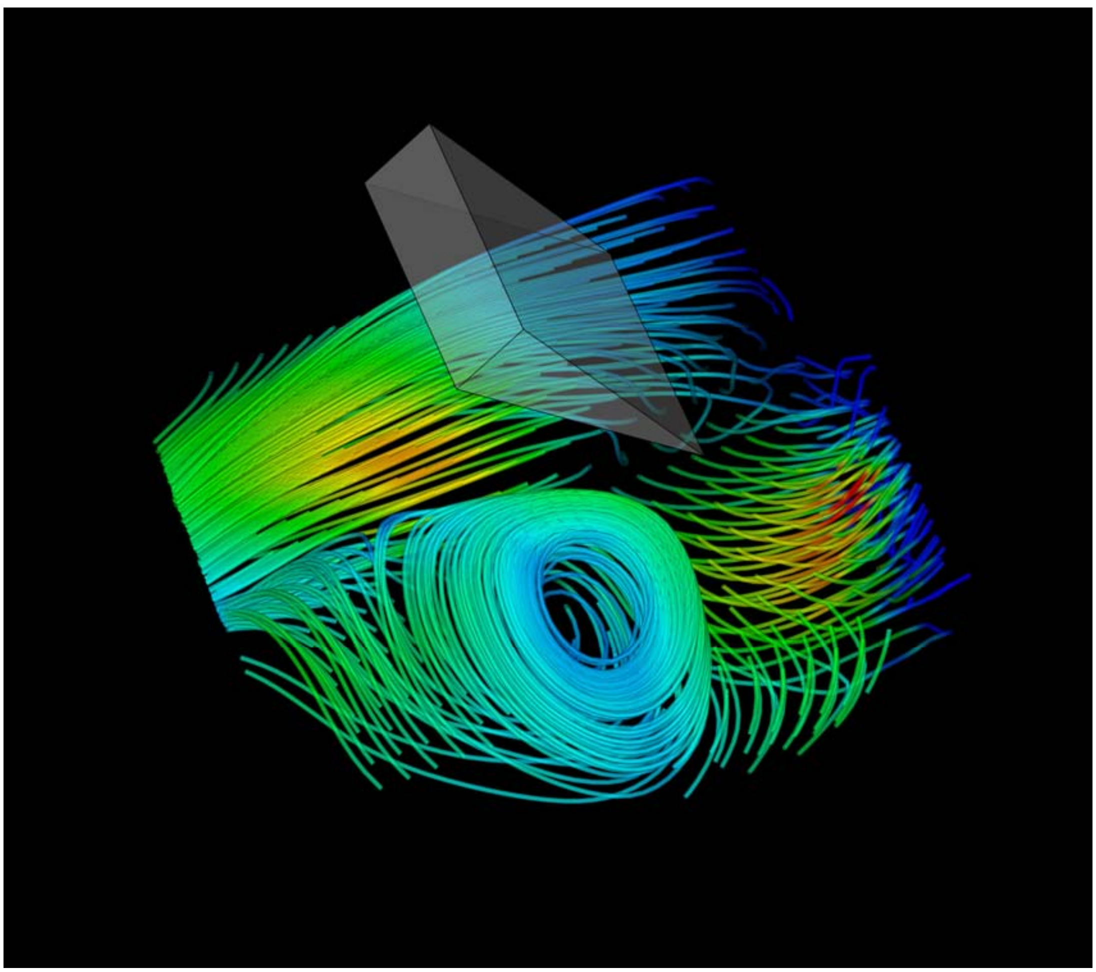

Figure 12: Velocity streamlines for one pair of point clouds with a model of the flap included according to the position indicated by the filtered point cloud. The flap is currently rotating toward the top left of the image.

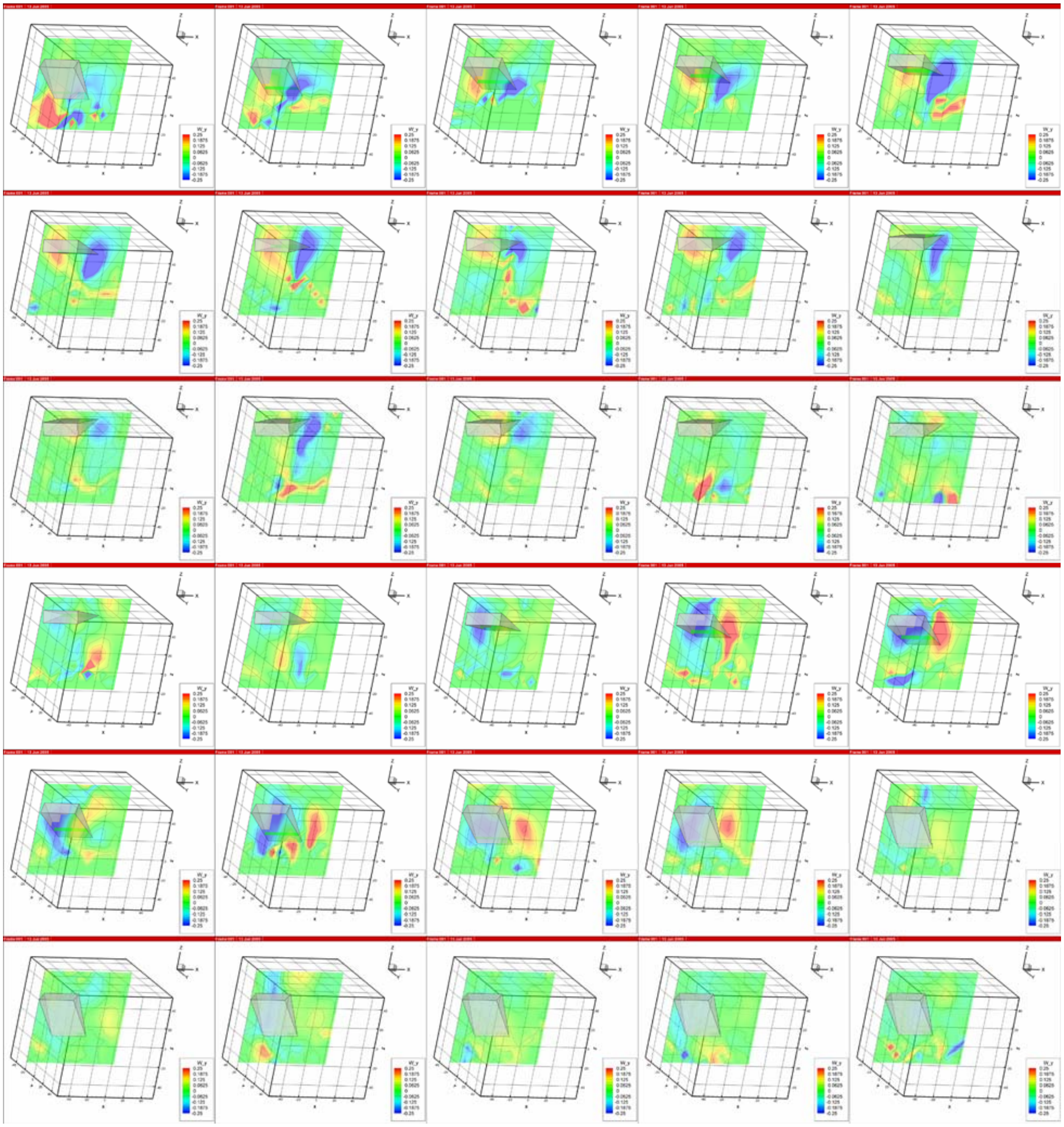

Figure 13: Vorticity slices for one stroke of the flap. Each image is the result of a single pair. The vorticity is calculated by finite difference; shown here is the Y-component. The slice is approximately 30% from the tip of the flap.

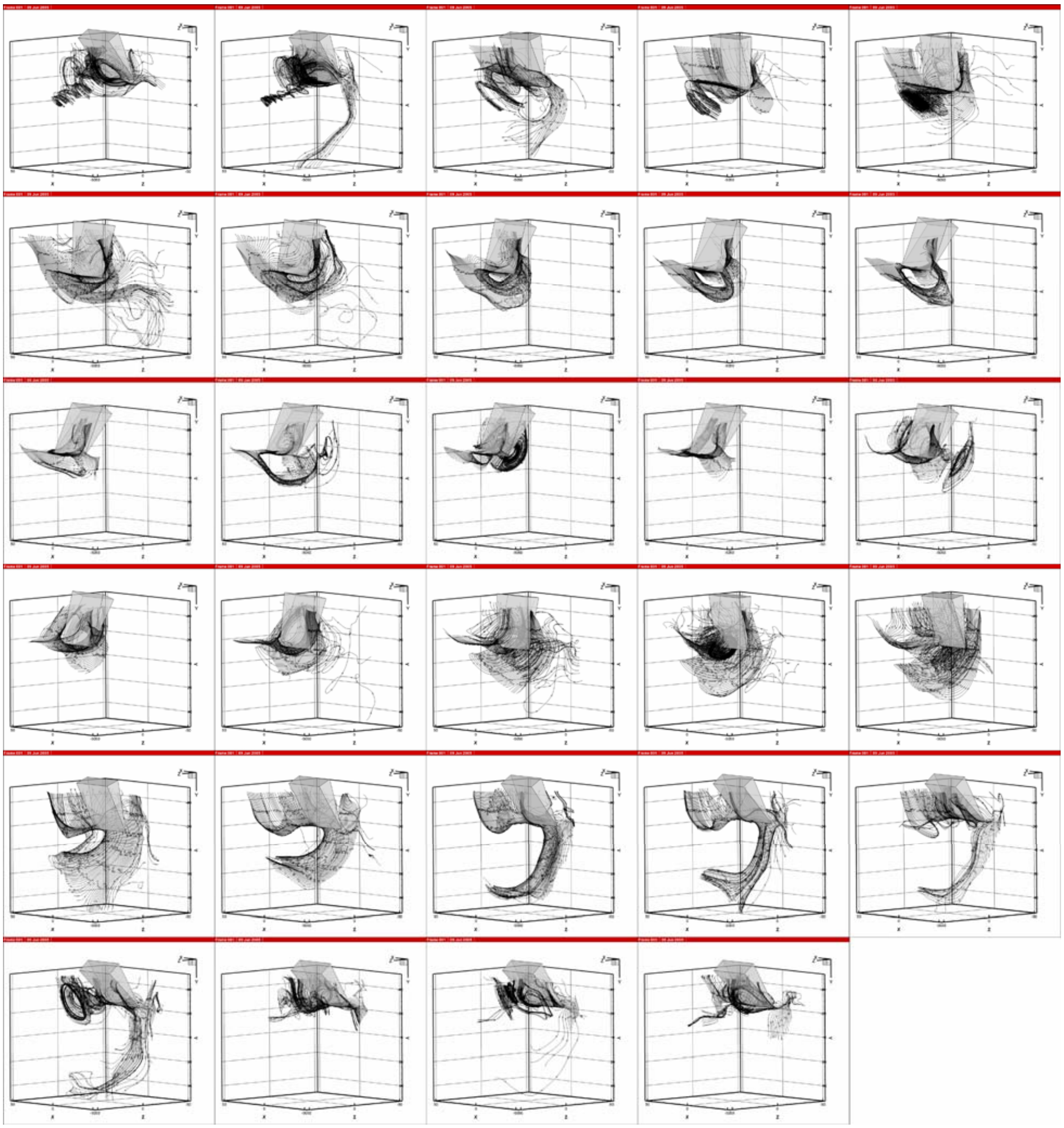

Figure 14: Vorticity streamlines for one flap cycle. The vorticity was calculated by finite differencing on a phase-averaged set (30 cycles). Of note are the corkscrew vortex on the corner of the plate and the strong core of vorticity formed directly around the flap during the cycle.

Piston-Cylinder Vortex Ring

A vortex ring in water generated by a piston-cylinder arrangement was imaged transverse to its direction of travel. The ring was imaged as it was about to impact the bottom wall of the tank. The characteristic volume for this experiment was approximately 100mm. The seeding particles were 44-micron-diameter white polyurethane. Illumination came from the same Nd:YAG arrangement. Velocity was calculated with PIV.

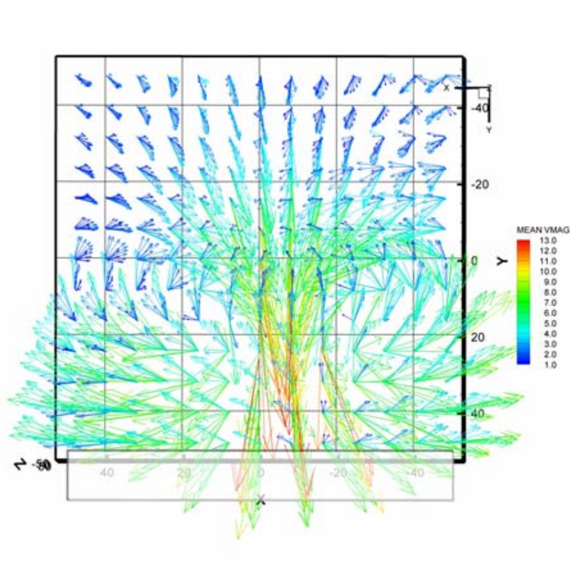

Figure 15: Vortex ring vectors for one pair of images. The white slab is the bottom of the tank.

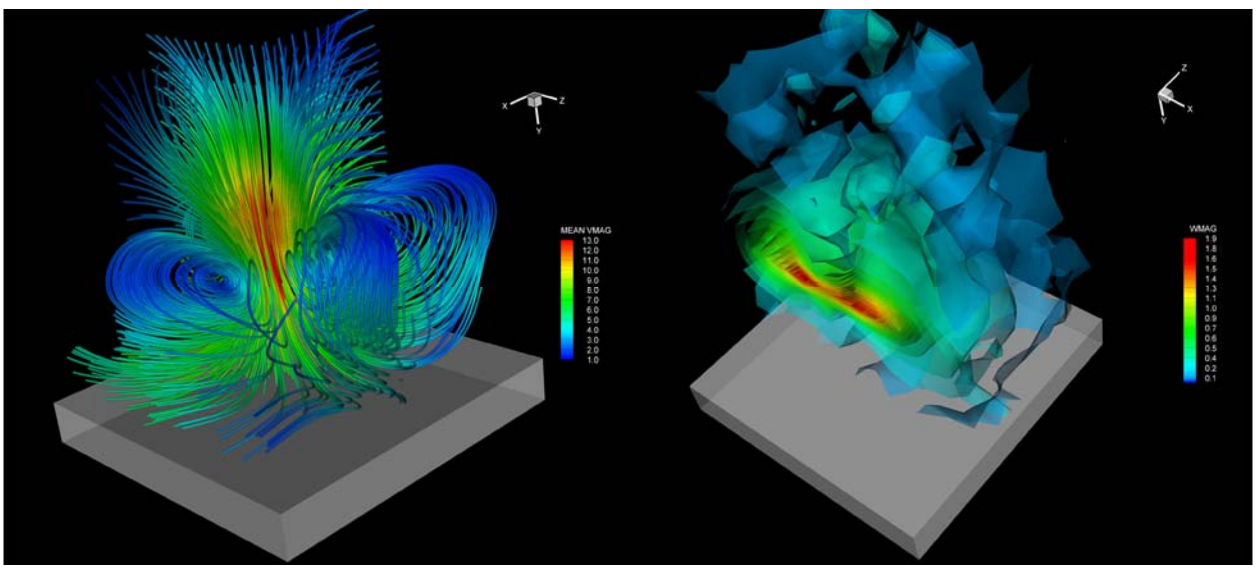

Figure 16: The same frame as above, visualized with velocity streamlines (left) and a section view of vorticity isosurfaces calculated by finite differencing (right). The grey slab is the bottom of the tank.

Particle Tracking Velocimetry

Translucent plastic particles (200-micron-diameter) slightly heavier than water were introduced at the free surface of the tank and through the course of the experiment drifted to the bottom of the tank. The slow flow lends itself well to particle tracking. In this case particle fields of more than 14,000 particles per frame (in a characteristic volume about 120mm) were tracked successfully.

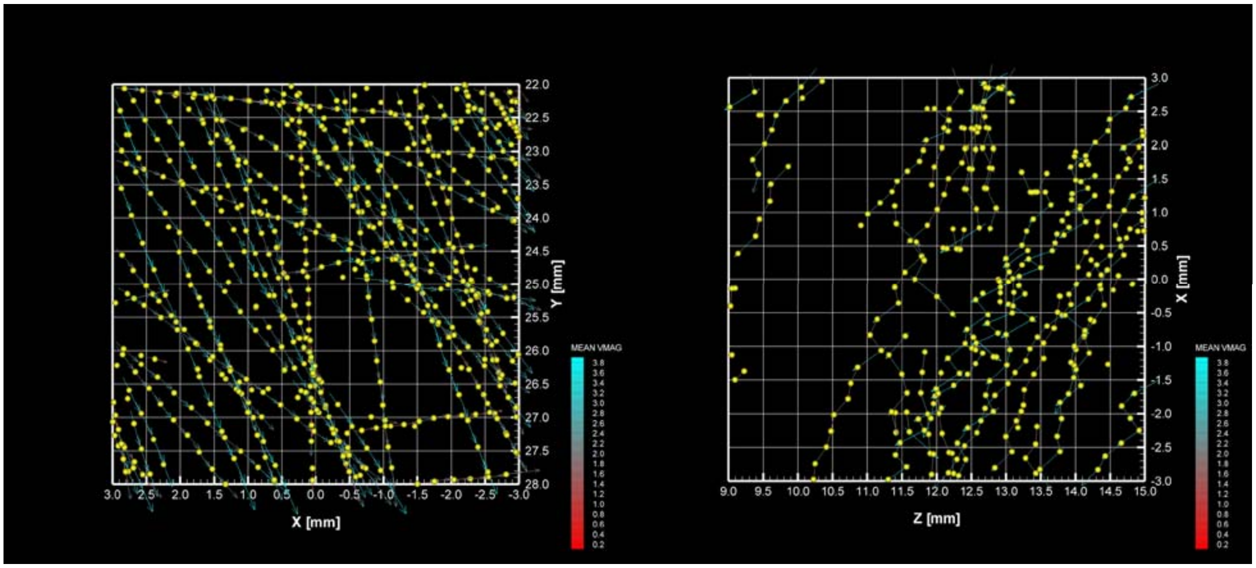

Figure 17: Detail of particle tracks of high-density particle tracking demonstration. This second-generation DDPIV camera (shown in figure 10) has an accuracy in X,Y of around 20 microns and in Z of about 140 microns. In these small sectional views of the particle fields, the distinction in the error is evident. Third-generation cameras should perform at least 2.5 times better in Z.

Piston-Cylinder Vortex Ring and a Bubble Plume

Here a bubble plume was generated by a standard aquarium air stone in a water tank that had already been seeded with 200-micron-diameter (mean) translucent plastic particles. Illumination came from a strobe in forward-scatter arrangement.

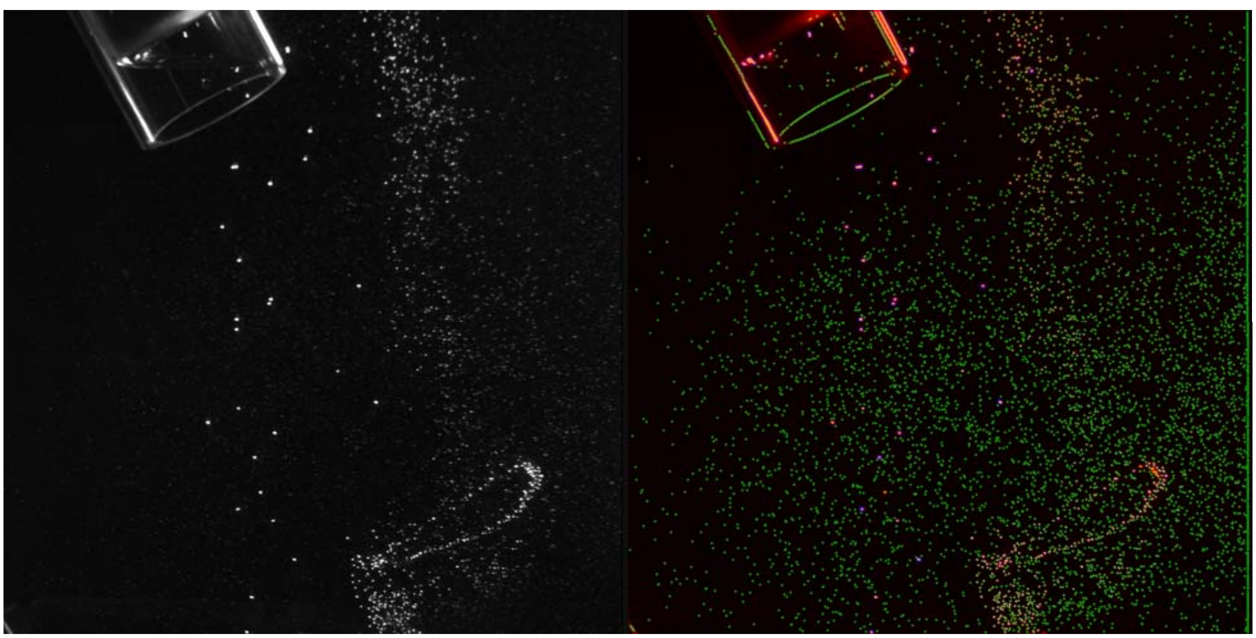

Figure 18: On the left is a raw image (from one sensor only) of the vortex ring bubble plume experiment. The faint grey spots are the plastic particles. Brighter images are from bubbles, including (just left of center) large bubbles coming from a leak in the stone's air fitting. Note also the cylinder clearly visible in the top left. On the right is the same raw image with the detected peaks superimposed.

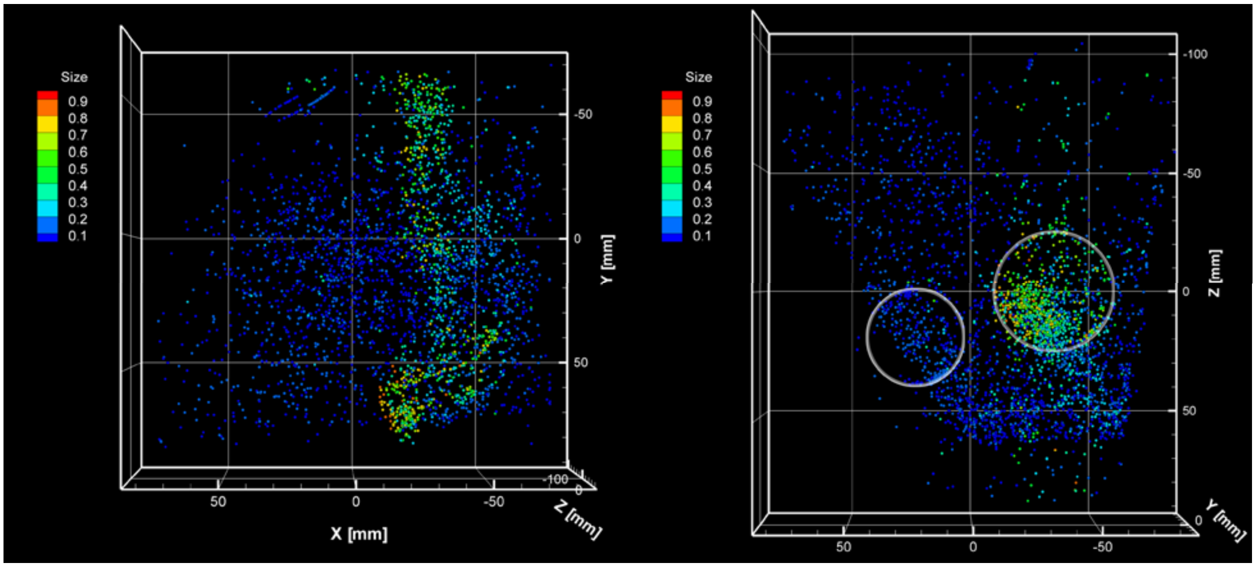

Figure 19: The frame from figure 18 processed into a point cloud. On the left is a view in the same orientation as the camera imaged the experiment. On the right is a view perpendicular to the imaging direction. The cylinder and vortex ring have been highlighted. The color scale for both images is relative particle size. Since no sizing calibration was performed, absolute size cannot be measured. This shows the clear difference in size between the bubbles and the plastic particles.

5 Conclusion

DDPIV is a true three-dimensional velocimetry technique that includes the ability to perform sizing of particles and surface tracking simultaneously with the velocity measurements. It has been applied to multiphase flows in the lab and in the field. Its precision with respect to other three-dimensional techniques is unmatched, especially considering its typically compact size.

The DDPIV technique is protected by US Patent 6,278,847. Its development is graciously supported by the Office of Naval Research (grant number N00014-97-1-0303).

References

Cho Y C (1989) Digital image velocimetry. Appl. Opt., 28, 740-8

Gauthier V; Riethmuller M L (1988) Application of PIDV to complex flows: measurements of the third component. Kármán institute for fluid mechanics – *Particle Image Displacement Velocimetry*. Belgium: Rhode-Saint-Genèse

Kähler C J; Kompenhans J (2000) Fundamentals of multiple plane stereo particle image velocimetry. Exp. Fluids 29, S070-7

Keane R D; Adrian R J (1992) Theory of cross-correlation analysis of PIV images. Appl. Sci. Res., 49, 191-215

Pereira F; Gharib M (2002) Defocusing digital particle image velocimetry and the three-dimensional characterization of two-phase flows. Meas. Sci. Technol., 13, 683-694

Pereira F; Gharib M (2004) A method for three-dimensional particle sizing in two-phase flows. Meas. Sci. Technol., 15, 2029-2038

Pereira F; Gharib M; Dabiri D; Modarress D (2000) Defocusing digital particle image velocimetry: a 3-component 3-dimensional DPIV measurement technique. Application to bubbly flows. Exp. Fluids, 29, S78-84

Prasad A K; Jensen K (1995) Scheimpflug stereocamera for particle image velocimetry in liquid flows. Appl. Opt., 34, 7092-9

Westerweel J (1997) Fundamentals of digital particle image velocimetry. Meas. Sci. Technol., 8, 1379-92

Willert C E; Gharib M (1991) Digital particle image velocimetry. Exp. Fluids, 10, 181-93